Received: 28 September 2023 | Revised: 9 January 2024 | Accepted: 28 January 2024

IET Systems Biology

DOI: 10.1049/syb2.12089

The Institution of Engineering and Technology WILEY

ORIGINAL RESEARCH

# Analysis of disulfidptosis- and cuproptosis-related LncRNAs in modulating the immune microenvironment and chemosensitivity in colon adenocarcinoma

Qiang Fan[1] | Guang-Bo Wu[1] | Min Chen[1] | Lei Zheng[1] | Hong-Jie Li[1] | Lv-Zhu Xiang[2] | Meng Luo[1]

[1]Department of General Surgery, Shanghai Ninth People's Hospital Affiliated to Shanghai Jiao Tong University School of Medicine, Shanghai, China

[2]State Key Laboratory of Systems Medicine for Cancer, Shanghai Cancer Institute, Renji Hospital, Shanghai Jiao Tong University School of Medicine, Shanghai, China

**Correspondence**

Lv-Zhu Xiang and Meng Luo, Shanghai Ninth People's Hospital Affiliated to Shanghai Jiao Tong University School of Medicine, No.639, Manufacturing bureau Road, Shanghai 200011, China.
Email: xianglvzhu@shsci.org and luosh9hospital@sina.com

**Funding information**

The Clinical Research Program of 9th People's Hospital, Shanghai Jiao Tong University School of Medicine, Grant/Award Number: JYLJ202124; National Outstanding Youth Science Fund Project of National Natural Science Foundation of China, Grant/Award Numbers: 81970526, 81900550, 82100639, 82200630; Fundamental research program funding of Ninth People's Hospital affiliated to Shanghai Jiao Tong university School of Medicine, Grant/Award Number: JYZZ162

**Abstract**

The main objective was to establish a prognostic model utilising long non-coding RNAs associated with disulfidptosis and cuproptosis. The data for RNA-Sequence and clinicopathological information of Colon adenocarcinoma (COAD) were acquired from The Cancer Genome Atlas. A prognostic model was constructed using Cox regression and the Least Absolute Shrinkage and Selection Operator method. The model's predictive ability was assessed through principal component analysis, Kaplan–Meier analysis, nomogram etc. The ability of identifying the rates of overall survival, infiltration of immune cells, and chemosensitivity was also explored. In vitro experiments were conducted for the validation of differential expression and function of lncRNAs. A disulfidptosis and cuproptosis-related lncRNA prognostic model was constructed. The prognostic model exhibits excellent independent predictive capability for patient outcomes. Based on the authors' model, the high-risk group exhibited higher tumour mutation burdened worse survival. Besides, differences in immune cell infiltration and responsiveness to chemotherapeutic medications exist among patients with different risk scores. Furthermore, aberrant expressions in certain lncRNAs have been validated in HCT116 cells. In particular, FENDRR and SNHG7 could affect the proliferation and migration of colorectal cancer cells. Our study developed a novel prognostic signature, providing valuable insights into prognosis, immune infiltration, and chemosensitivity in COAD patients.

**KEYWORDS**

bioinformatics, cancer

## 1 | INTRODUCTION

Based on the information provided by the World Health Organisation, it is estimated that around 1.4 million individuals succumb to adenocarcinomas of the oesophagus, stomach, colon, or rectum annually on a global scale (https://www.who.int/news-room/fact-sheets/detail/cancer). Colon adenocarcinoma (COAD) is the most common histological subtype of colon carcinoma, accounting for more than 90% of cases and linked to a grim prognosis [1, 2]. Over the past few years, there has been a rise in the occurrence rates of COAD, accompanied by a gradual change in the disease's risk towards younger age groups [3]. The treatment choices for COAD vary based on the disease stage and can involve surgical procedures, chemotherapy, radiation therapy, and targeted therapy. The use of immunotherapy in colorectal adenocarcinoma is still being investigated [4]. Nevertheless, so far, the commonly employed

Qiang Fan, Guang-Bo Wu and Min Chen contributed equally to this work.

staging methods have provided somewhat inaccurate forecasts for therapeutic choices and outcomes in individuals with COAD [5]. Therefore, it is essential to discover novel predictive biomarkers and tumour markers to accurately predict the amelioration and overall survival (OS) of individuals with COAD.

Disulfidptosis, a term coined to describe cell death induced by disulfide stress, displays unique features compared to other types of regulated cell death [6]. There is increasing evidence suggesting a strong connection between the abnormal buildup of intracellular disulfides, such as cysteine, and tumour cell metabolism [7–9]. This accumulation of disulfides resulted in disulfide stress, which posed a significant risk to cellular homoeostasis and cell survival. To combat this stress, the essential reducing power was supplied by the nicotinamide adenine dinucleotide phosphate (NADPH). The NADPH pool was depleted when glucose starvation was combined with this process, leading to the accumulation of intracellular disulfides and causing rapid cell death [10]. NADPH is mainly synthesised through glucose metabolism, and under conditions of glucose deprivation within cancer cells, it can initiate disulfidptosis specific to cancer cells [11]. Therefore, glycolysis plays a crucial role in cancer, not only providing energy and building blocks for tumour cell synthesis but also closely associated with the initiation of different cell death pathways in tumour cells.

Cuproptosis is another type of cell death process that is closely associated with mitochondrial respiration and affected by protein lipoylation. It has been implicated in various diseases, including COAD [12]. Notably, a recent study has provided evidence for the involvement of cuproptosis in the progression of colorectal cancer. It revealed that the inhibition of glycolysis promotes cuproptosis, highlighting its potential as a promising therapeutic strategy for the treatment of colorectal cancer [13]. Research findings have indicated that the products generated through glycolysis have the capacity to modulate the activity of disulfidptosis and cuproptosis pathways, ultimately influencing the fate of tumour cells [14, 15]. Given the intricate correlation between programmed cell death (disulfidptosis and cuproptosis) and glucose metabolism, we decided to explore the potential interaction between disulfidptosis- and cuproptosis-related lncRNAs in the pathogenesis of COAD.

Our study obtained clinical information of individuals diagnosed with COAD and RNA-Sequence data from the Cancer Genome Atlas (TCGA) database. The information was used to establish and verify a predictive model for COAD using disulfidptosis- and cuproptosis-related lncRNAs. Furthermore, several bioinformatic investigations were conducted to explore the expression of disulfidptosis- and cuproptosis-related lncRNAs and their potential influence on the progression of COAD. These analyses included the examination of infiltrating immune cells, gene set enrichment analysis (GSEA), immune checkpoints, and chemotherapy drug analysis. In addition, in vitro experiments confirmed the differences in the expression levels of these lncRNAs and explored the effects on the proliferation and migration of colorectal cancer cells. Our results facilitated in investigating potential biomarkers that could be used as new targets for prognosis and treatment of COAD.

## 2 | METHODS

### 2.1 | Data acquisition

The RNA-Sequence data and corresponding clinicopathological data of COAD were acquired from TCGA, whose website is https://portal.gdc.cancer.gov. We obtained and merged transcriptome profiles of 517 samples, which included 476 samples with cancer and 41 samples that were normal. The sequencing data were subsequently annotated using human gene annotation files from the Ensembl official website (http://asia.ensembl.org/index.html).

### 2.2 | Identification of disulfidptosis- and cuproptosis-related lncRNAs

The identification of lncRNAs related to disulfidptosis and cuproptosis involved the calculation of the correlation coefficient between the expression levels of genes and the expression levels of lncRNAs. The disulfidptosis- and cuproptosis-related genes were depicted in Table 1. The selection process involved setting the filter criteria as $|\text{Pearson } r| > 0.4$ and $p < 0.001$ and choosing the lncRNAs that satisfied the criteria. Here, a total of 1309 lncRNAs associated with disulfidptosis and cuproptosis were collectively identified. Subsequently, we integrated clinical data from tumour samples to perform survival analysis and Univariate Cox regression analysis, leading to the identification of 109 lncRNAs significantly associated with the prognosis of cancer patients. Differential expression analysis of these lncRNAs in normal samples and tumour samples from TCGA dataset was conducted, with criteria set at a $|\text{LogFC}| > 1$ and a false discovery rate (FDR) of less than 0.05. All 109 identified lncRNAs met the selection criteria and were further employed in subsequent analyses.

### 2.3 | Construction and validation of the prognostic model

In order to avoid overfitting, we employed the least absolute shrinkage and selection operator (Lasso) method to choose the lncRNAs for model construction. The penalty parameter ($\lambda$) was fine-tuned through cross-validation. During our research, we identified 8 lncRNAs with a prognostic value, which were selected to build a model and further enhanced through cross-validation. The risk score for every patient was calculated using the formula: $\sum N\ i\ =\ 1(\text{Coef}_i{*}X_i)$, where $\text{Coef}_i$ denoted the coefficient derived from the Cox

**TABLE 1** List of disulfidptosis- and cuproptosis -related genes.

| Gene |
|---|
| SLC7A11 |
| GYS1 |
| NDUFS1 |
| NDUFA11 |
| NUBPL |
| NCKAP1 |
| LRPPRC |
| SLC3A2 |
| RPN1 |
| ACTN4 |
| ACTB |
| CD2AP |
| CAPZB |
| DSTN |
| FLNA |
| FLNB |
| INF2 |
| IQGAP1 |
| MYH10 |
| MYL6 |
| MYH9 |
| PDLIM1 |
| TLN1 |
| NFE2L2 |
| NLRP3 |
| ATP7B |
| ATP7A |
| SLC31A1 |
| FDX1 |
| LIAS |
| LIPT1 |
| LIPT2 |
| DLD |
| DLAT |
| PDHA1 |
| PDHB |
| MTF1 |
| GLS |
| CDKN2A |
| DBT |
| GCSH |
| DLST |

regression model and corresponding lncRNAs, and $X_i$ represented the expression levels of the lncRNAs. The COAD samples were categorised into high-risk (≥median) and low-risk (<median) groups based on the median risk score. R packages 'pheatmap' and 'ggbiplot' were introduced to perform T-Distributed stochastic neighbour embedding (*t*-SNE), Principal Component Analysis (PCA), and the corresponding survival visualisation analysis. The R packages 'survival' and 'survminer' were introduced for Kaplan–Meier (K–M) survival curve analysis in order to compare the survival rates of low- and high-risk groups. We also conducted the R package 'timeROC' to perform ROC curve analysis, which was dependent on time, in order to evaluate the predictive precision of this signature. The AUCs were computed at 1, 3, and 5 years, respectively. To assess the reliability of the 8 lncRNAs signature in patients with varying clinical characteristics, K–M plots were conducted as well.

## 2.4 | Construction of gene set enrichment analysis

Here, we introduced GSEA by GSEA 4.0.1 software in order to investigate the Kyoto Encyclopaedia of Genes and Genomes pathways between the low- and high-risk groups. A filter criteria of $p < 0.05$ and FDR <5% was also performed in this analysis.

## 2.5 | Analysis of somatic variants and tumour mutation burden (TMB)

The TCGA database provided the somatic mutation data for the samples in a VarScan file format. To determine the significant mutated genes and tumour mutation burden (TMB) for the high- and low-risk groups, the R package 'maftool' was employed in this study. The R packages of 'Survival, ggpubr and reshape2' were utilised to analyse the variation in survival outcomes and TMB between high- and low-risk groups.

## 2.6 | Investigation of the immune infiltration

Aiming to examine the association between immune cell infiltration and the expression of 8 lncRNAs, various techniques and programs, including XCELL, TIMER, QUANTISEQ, MCPCOUNTER, EPIC, CIBERSORT-ABS, and CIBERSORT, were employed to measure the abundance of infiltrating immune cells in COAD patients from TCGA. Afterwards, ssGSEA was introduced in with the help of R packages ('reshape2' and 'ggpubr') to measure the presence of immune cells and functions related to immunity, as well as investigate the immune connection between low- and high-risk groups. Furthermore, R packages ('ggplot2' and 'ggpubr') were utilised to perform immune checkpoint analysis, aiming to compare the levels of immune checkpoints expression in low- and high-risk groups.

## 2.7 | Evaluation of chemotherapeutic drug sensitivity

To evaluate the responsiveness of chemotherapy drugs in the two categories, we introduced in and utilised the pRRophetic R package, which was obtained from the GitHub repository 'https://github.com/paulgeeleher/pRRophetic', to forecast the IC50 (half-maximal inhibitory concentration) of chemotherapy drugs for each patient classified into low and high-risk groups. In view of the screening of a plethora of chemotherapeutic drugs based on 8 lncRNAs, we selected 12 clinically approved drugs for subsequent investigation.

## 2.8 | Consensus clustering for disulfidptosis and cuproptosis-related lncRNAs

Consensus clustering analysis was conducted on 8 lncRNAs using the R package 'ConsensusClusterPlus'. To determine the best balance between stability and informativeness for every cluster, the assessment involved comparing the similarity of levels of prognostic lncRNA and the proportion of fuzzy similarity measurements. Similar techniques, such as the K–M survival curve, Sankey diagram, PCA, t-SNE, immune infiltration, immune checkpoints, and sensitivity, were introduced in to analyse the chemotherapeutic agents.

## 2.9 | Construction of nomogram

In order to rigorously validate the model and anticipate its clinical application in the future, we integrated the model with clinical data from TCGA. Here, we incorporated risk scores with age, stage, and metastasis, utilising the rma R package to construct a nomogram. Additionally, we employed calibration curves at 1-, 2-, and 3-year timeframes to assess the accuracy of the nomogram.

## 2.10 | Cell lines and transfection

The HCT116 cell line, which was a type of Human COAD cell, were acquired from the Chinese Academy of Medical Sciences located in Beijing, China. NCM460, which was a type of Human normal colon cells, were acquired from there as well. The HCT116 cells were grown in McCoy's 5A solution (Gibco) with the addition of 10% Foetal Bovine Serum (Life Technologies, Inc.) and 1% penicillin-streptomycin (Gibco) under 5% $CO_2$ and 37 °C in a humidified incubator. We cultured the NCM460 cells in RPMI-1640 medium (Gibco) supplemented with 10% Foetal Bovine Serum (Life Technologies, Inc.) at 37 °C in a humidified atmosphere containing 5% $CO_2$. Meanwhile, we purchased GenePharma (Shanghai, China) the products of the scrambled siRNA of SNHG7 or AP003555.1 (siControl) and specific siRNAs targeting SNHG7 (siSNHG7) and AP003555.1 (siAP003555.1), as well as pcDNA3.1-Control (pcDNA/Control), pcDNA3.1-SNHG7 (pcDNA/SNHG7), and pcDNA3.1-AP003555.1 (pcDNA/AP003555.1). Cell transfection was performed using Lipofectamine 2000 Reagents from Invitrogen Co., located in Carlsbad, CA, USA, following the guidelines provided by the manufacturer. The pLVX-EF1a-IRES-Puro plasmid (Clontech) was used to create a lentiviral vector that amplifies the lncRNA FENDRR through subcloning of the FENDRR cDNA sequence. The plasmid was transfected with the help of ExFect Transfection Reagent (Vazyme, China) according to the instructions provided by the manufacturer. Afterwards, the HCT116 cells were chosen under the treatment of puromycin.

## 2.11 | CCK-8 assay

HCT116 cells were plated in 96-well plates with a concentration of $1 \times 10^4$ cells/mL and volume of 100 μL per well. At 0, 24, 48, and 72 h, the viability of the cells was evaluated after the cells adhered completely. In each well, 10 μL of a CCK-8 reagent from Vazyme in China were added, and the cells were then incubated at 37°C for a duration of 2 h. The Synergy two enzyme-labelling instrument (BioTek) was utilised to measure the absorbance at 450 nm.

## 2.12 | Cell migration

HCT116 cells were placed in 60-mm cell culture dishes and grown until they reached complete confluence. Using a micropipette tip with a volume of 200 μL, a clear wound was made in the confluent monolayer. Afterwards, the cells were rinsed using phosphate-buffered saline in order to eliminate any cells that had become detached. To record the marks on every plate, microscopic pictures were taken. For the purpose of reducing the influence of DNA replication and proliferation on the rate of cell migration, the current experiment utilised a medium without serum. The monitoring of the wound edge movement was conducted for a period of 24 h. Image J software was used to measure the space between the two edges of the scratch. To calculate the rate of cellular migration, we determine the relative area between the two sides of the scratch, and the following formula was used: cell migration rate = (scratch area at 0 h—scratch area at 24 h)/(scratch area at 0 h) × 100%.

## 2.13 | Colony formation assay

Around one thousand cells in each group were introduced into the specifications of 60-mm cell culture dishes and incubated for a duration of 14 days. The cells were treated with 4% paraformaldehyde for 15 min and then subjected to staining with 0.1% crystal violet for a duration of 20 min. Image J

software was used to determine the count of colonies that were visibly stained.

## 2.14 | Quantitative real-time PCR (qRT-PCR)

Total RNA was extracted with the help of a TRIzol reagent (Invitrogen). Following that, *r* reverse transcription was performed utilising a PrimeScript RT reagent Kit (Perfect Real Time; TaKaRa) according to the manufacturer's guidelines. We detected the presence of chosen lncRNAs with the help of Quantitative real-time PCR (qRT-PCR) and ABI Power SYBR Green PCR Master Mix (ABI, USA). The mRNA of glyceraldehyde 3-phosphate dehydrogenase (GAPDH) was chosen as a reference for internal control. The primer sequences were further depicted in Table 2. The levels of lncRNAs were presented as a fold alteration utilising the $2^{-\Delta\Delta Ct}$ approach and subsequently analysed.

## 2.15 | Statistical analyses

We performed the statistical analyses by R version 4.2.1, with a pre-established level of statistical significance defined as $p < 0.05$.

# 3 | RESULTS

## 3.1 | Screening for prognostic disulfidptosis- and cuproptosis-related lncRNAs

According to the analysis of the TCGA dataset, we identified 1309 lncRNAs which were significantly related to disulfidptosis and cuproptosis. The differential expression of lncRNAs between the normal and COAD samples was shown in the heatmap (Figure S1). Following this, a univariate Cox regression analysis was conducted, revealing a robust correlation between 107 lncRNAs and the OS of COAD (Figure 1a). In addition, 8

**TABLE 2** Sequence of primers for quantitative reverse transcription-PCR.

| Gene | Forward primer (5'------3') | Reverse primer (5'------3') |
|---|---|---|
| SNHG7 | GTGTGTCCCTTGGTGGAGAG | TCCCAGATACCAGCGAAGGA |
| FENDRR | AGACAAAAACTCACTGCCCA | TGATGTTCTCCTTCTTGCCTC |
| AL513550.1 | TCTCTCAGATCCATTTCCTAAGCC | AGTCTCCCTCATAGCCCTGTT |
| ATP2A1-AS1 | CGCACCAGGAGGTCTTCAAA | AGCCACAAAGTCTTGGGTGT |
| LINC01235 | GTCTCTCACAGGTCAACGCA | CCACGTCAAGGCTCCTCAAT |
| AL138756.1 | AAAGTGAGTTCAGTGCTGCC | CCAGCTCCCTGAAAGACGTA |
| AC002091.2 | GTCGTCTTCTCCCCAGTGATG | GTCTATGCTGGAGGAGCCAAA |
| AP003555.1 | CAGGGGGATGAGGGTACAGA | AACACCTGTAGTGACAGCGG |
| GAPDH | TGACTTCAACAGCGACACCCA | CACCCTGTTGCTGTAGCCAAA |

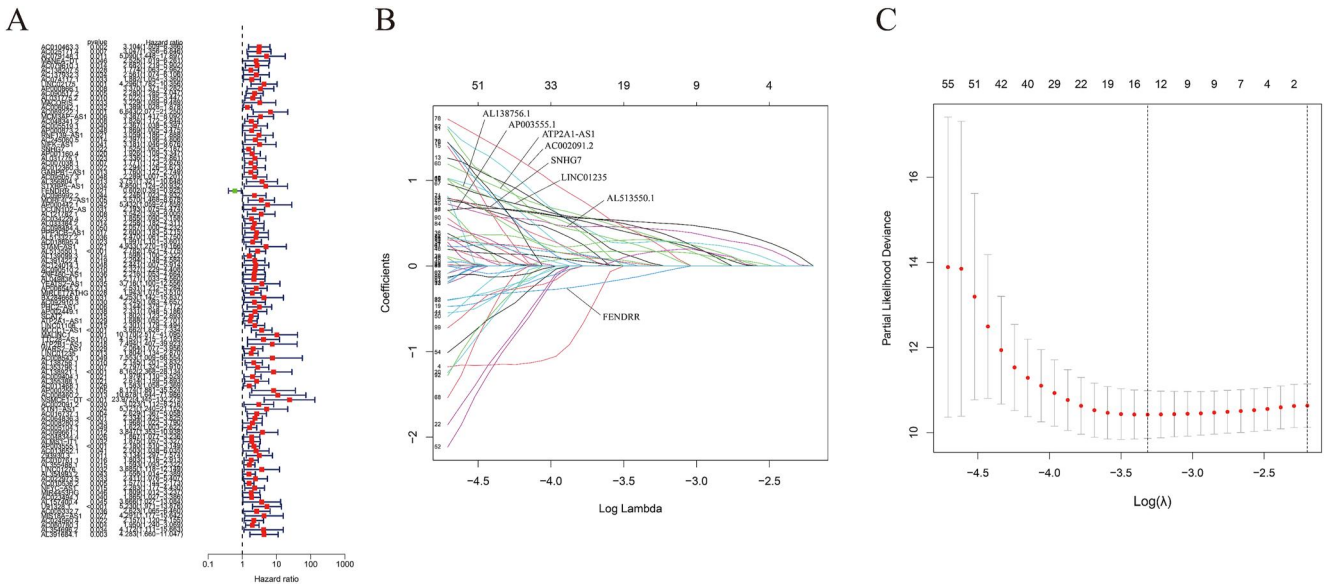


**FIGURE 1** Identification of prognostic disulfidptosis-related lncRNAs. (a) The results of univariate Cox regression analysis of prognosis-related lncRNAs. (b) LASSO coefficient profile of prognosis-related lncRNAs. (c) Partial likelihood deviance for different numbers of variables. (***$p < 0.001$, **$p < 0.01$, *$p < 0.05$).

prognostic lncRNAs (SNHG7, FENDRR, AL513550.1, ATP2A1-AS1, LINC01235, AL138756.1, AC002091.2, and AP003555.1) were identified to establish a prognosis model by using LASSO Cox regression analysis (Figures 1b,c).

### 3.2 | Assessment of disulfidptosis- and cuproptosis-related prognostic model based on 8 prognostic lncRNAs

According to the expression of the 8 lncRNAs, we could divide the individuals into low- or high-risk groups. The formula, risk score = 0.755,074,261,352,201 −0.366,338,080,197,758 * FENDRR + 0.827,016,266,555,419 * AL513550.1 + 0.839,898,867,767,624 * 'ATP2A1-AS1' + 1.03,111,831,808,473 * LINC01235 + 1.18,822,152,354,959 * AL138756.1 + 1.26,516,982,559,828 * AC002091.2 + 0.743,714,558,206,511 * AP003555.1, was performed to calculate the risk score of each patient. In the TCGA, training, and test cohorts, all patients were categorised into high- and low-risk groups, as depicted in Figures 2a–c. In addition, the median risk score also facilitated the categorisation of patients in the TCGA, training, and test cohorts into groups with high or low risk (Figures 2d–f). Moreover, in both the TCGA dataset and the training and test cohorts, the scatter plots revealed that patients in the high-risk group had a worse prognosis in comparison to those in the low-risk group, as evidenced by the denser red spots in the high-risk areas (Figures 2g–i).

### 3.3 | Prognostic significance of the 8 lncRNAs prognostic model

As expected, patients with higher risk scores in both the TCGA and training groups exhibited a shorter OS compared to those with lower risk scores. This finding was further confirmed in the test cohort (Figures 3a–c). The prognostic prediction of each variable was assessed using Univariate Cox proportional hazards regression analyses (HR = 1.050; CI = 1.031–1.070; $p < 0.001$) and Multivariate survival analyses (HR = 1.036; CI = 1.014–1.059; $p = 0.001$) (Figures 3d,e). In addition, the area under ROC (AUC) of various clinical characteristics also validated that the risk score exhibited a greater predictive value (AUC = 0.740) in comparison to conventional features such as Age, Gender, and Stage (Figure 3f). Subsequently, time-dependent ROC analysis was then employed to assess the prognostic capability of the risk score in patients with COAD. As shown in Figure 3g, the AUC values for 1, 3, and 5 years were 0.686, 0.740, and 0.764, respectively.

### 3.4 | Clinical significance of the 8 lncRNAs prognostic model

To further investigate the clinical significance of the prognostic model for lncRNAs in patients with COAD, we categorised the patients into various subgroups based on age, gender, and TNM staging system. The survival rates of individuals were analysed using K–M survival analysis, resulting in the generation of K–M survival curves within different subgroups. The findings suggested that, with the exception of patients in the T1-2 subgroup, the survival probabilities of patients in the high-risk group in each subgroup was significantly worse than those of patients in the low-risk group (Figures 4a–l). Therefore, the prognosis model of lncRNAs showed a significant prognostic value in predicting the survival rate of colorectal cancer.

### 3.5 | Functional enrichment analysis in high- and low-risk groups

The differentially expressed genes (DEGs) analysis was conducted to compare the gene expression of the low-risk group with that of the high-risk groups. The heatmap (Figure 5a) showed a total of 30 significant DEGs. DEGs were exhibited in the expression matrix of the volcanic plots, with the upregulated genes represented by green plots (Figure 5b). Subsequently, Gene ontology (GO) enrichment analysis of DEGs in two groups was carried out. The results were depicted in Figures 5c,d, including the three GO categories biological process, cellular component, and molecular function. Furthermore, GSEA was employed to investigate the differences between the patients in low- and high-risk groups. The findings indicated that in the low-risk group, there was enrichment of signalling pathways like Epidermal cell differentiation, Epidermis development, Keratinisation and Keratinocyte differentiation. Conversely, in the high-risk group, there was a significant enrichment of signalling pathways such as Chromatin remodelling, DNA replication dependent chromatin assembly, Nucleosome assembly, Nucleosome organisation and Protein DNA complex subunit organisation (Figures 5e,f).

### 3.6 | Analysis of somatic variants and evaluation of tumour mutation burden (TMB)

Tumour genomic features are of interest due to their impact on the tumour microenvironment and immunotherapy. Through somatic variant analysis, mutations in most genes were identified in both high- and low-risk groups. Figures 6a, b illustrated the top 20 mutated genes in the high- and low-risk groups, with 97.45% and 94.5%, respectively. Furthermore, the high-risk group exhibited a significantly higher TMB compared to the low-risk group (Figures 6c,d). Additionally, patients with high TMB had poorer survival probabilities compared to those with low TMB (Figure 6e). It was worth noting that within the high- and low-TMB subgroups, the low-risk group demonstrated better survival probabilities than the high-risk group (Figure 6f).

### 3.7 | Tumour immune cell infiltration and gene expression

To investigate the potential association between the immune infiltration microenvironment and risk scores, seven software

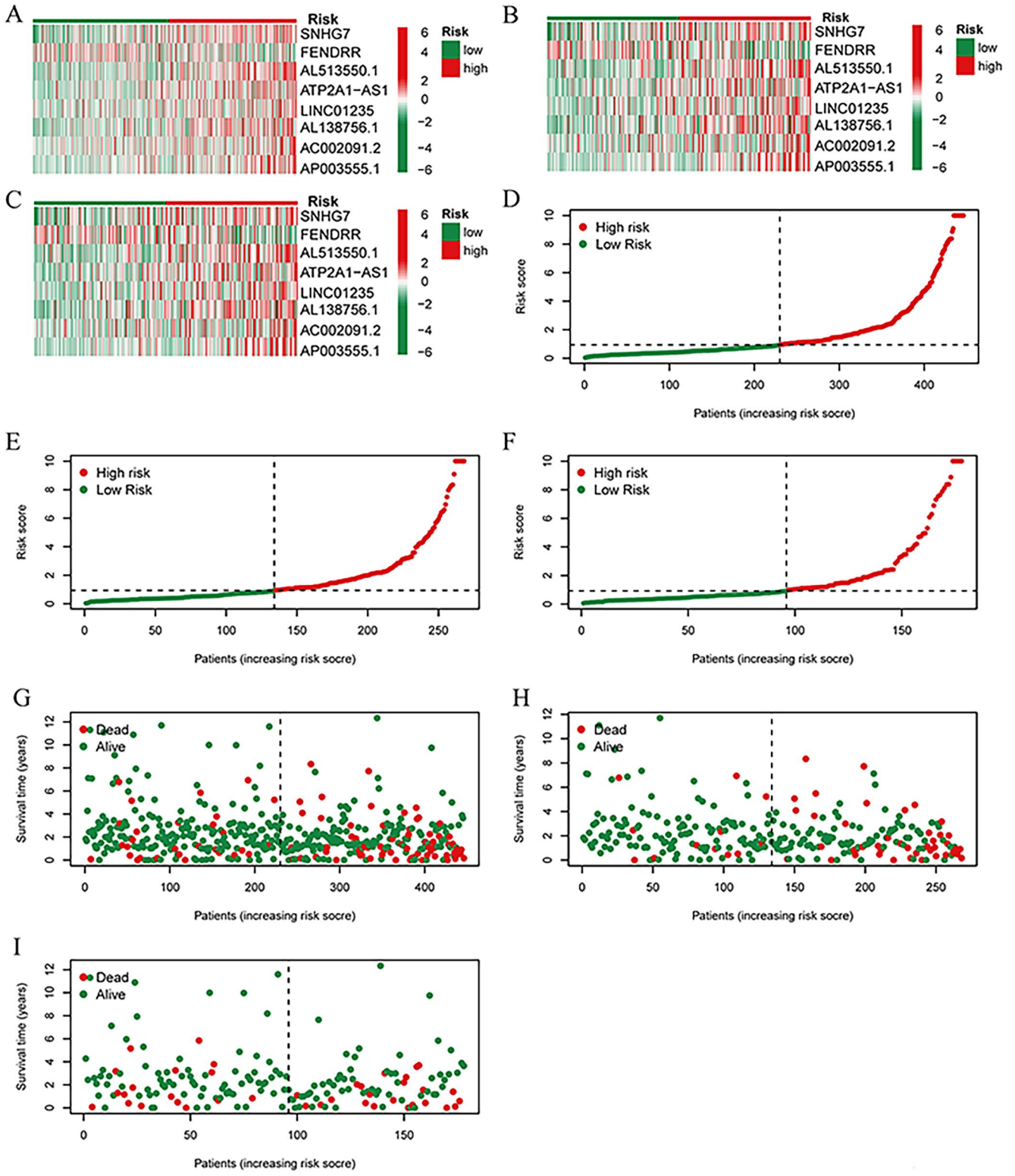


**FIGURE 2** Construction of the disulfidptosis-related prognosis model. (a–c) The heatmaps of the 8 prognostic lncRNAs in TCGA dataset, training cohort and testing cohort. (d–f) The median value and distribution of the risk scores in TCGA dataset, training cohort and testing cohort. (g–i) The distribution of survival time and status in TCGA dataset, training cohort and testing cohort. TCGA, the cancer Genome Atlas.

programmes (XCELL, TIMER, QUANTISEQ, MCPCOUNTER, EPIC, CIBERSORT-ABS, and CIBERSORT) were employed for analysing the correlation between infiltrated immune cells and risk scores. The majority of T cells, macrophages, B cells, natural killer cells (NK cells), mast cells, and other immune cells exhibited consistent trends with increased patient risk scores (Figure 7a). Notably, CIBERSORT-ABS and CIBERSORT analyses revealed that

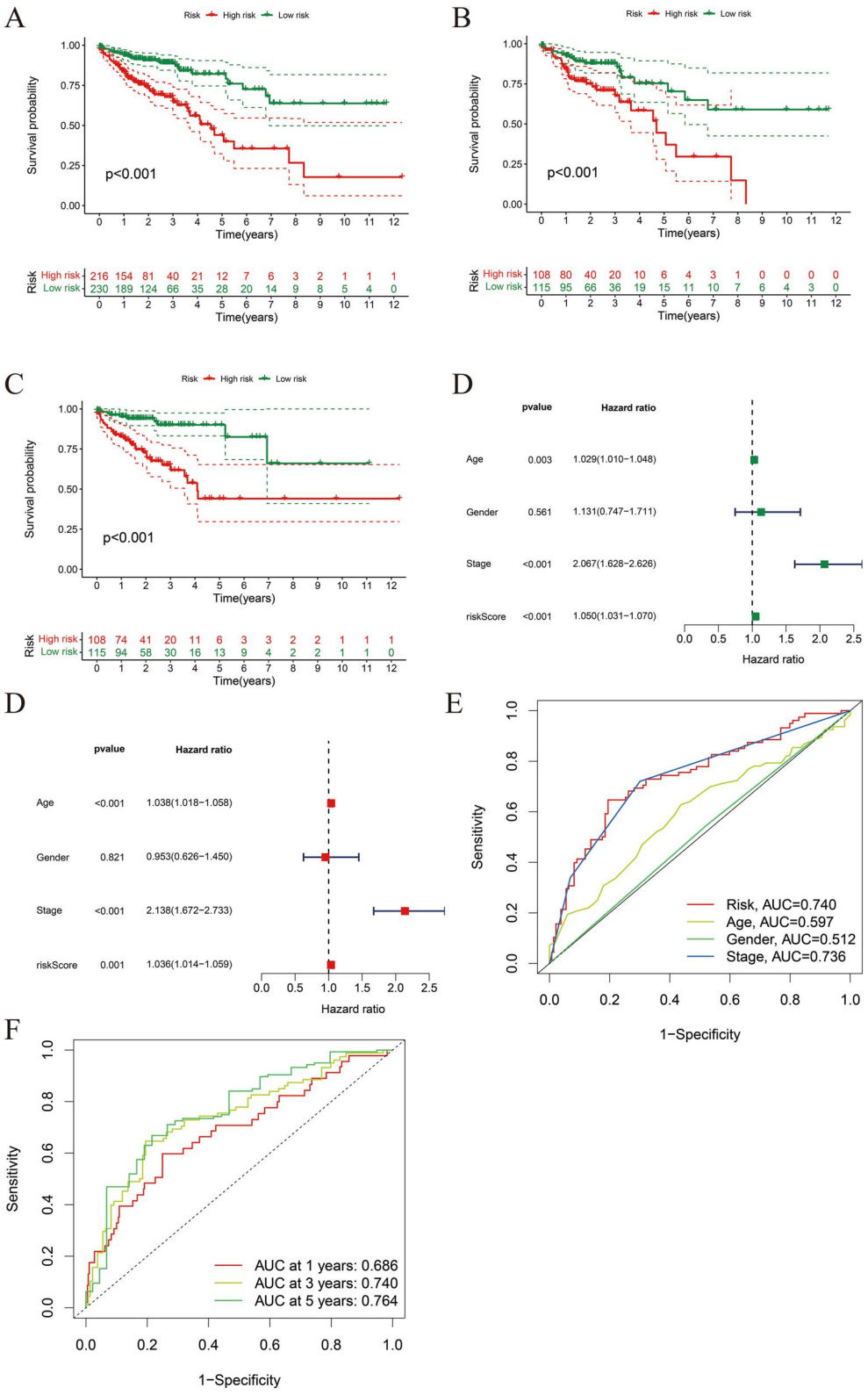


**FIGURE 3** lncRNAs signature predicted the efficiency of OS in patients with COAD. (a–c) Kaplan–Meier curves for OS of patients in the high- and low-risk groups in TCGA dataset, training cohort and testing cohort. (d) Univariate Cox regression analysis was performed to identify OS-related factors in the TCGA dataset. (e) Multivariate Cox regression analysis was conducted to screen for OS-related factors in the TCGA dataset. (f) AUC time-dependent ROC curves for different clinical features in the TCGA dataset. (g) AUC time-dependent ROC curves for OS at 1, 3 and 5 years in the TCGA dataset. COAD, Colon adenocarcinoma; OS, overall survival; TCGA, the cancer Genome Atlas.

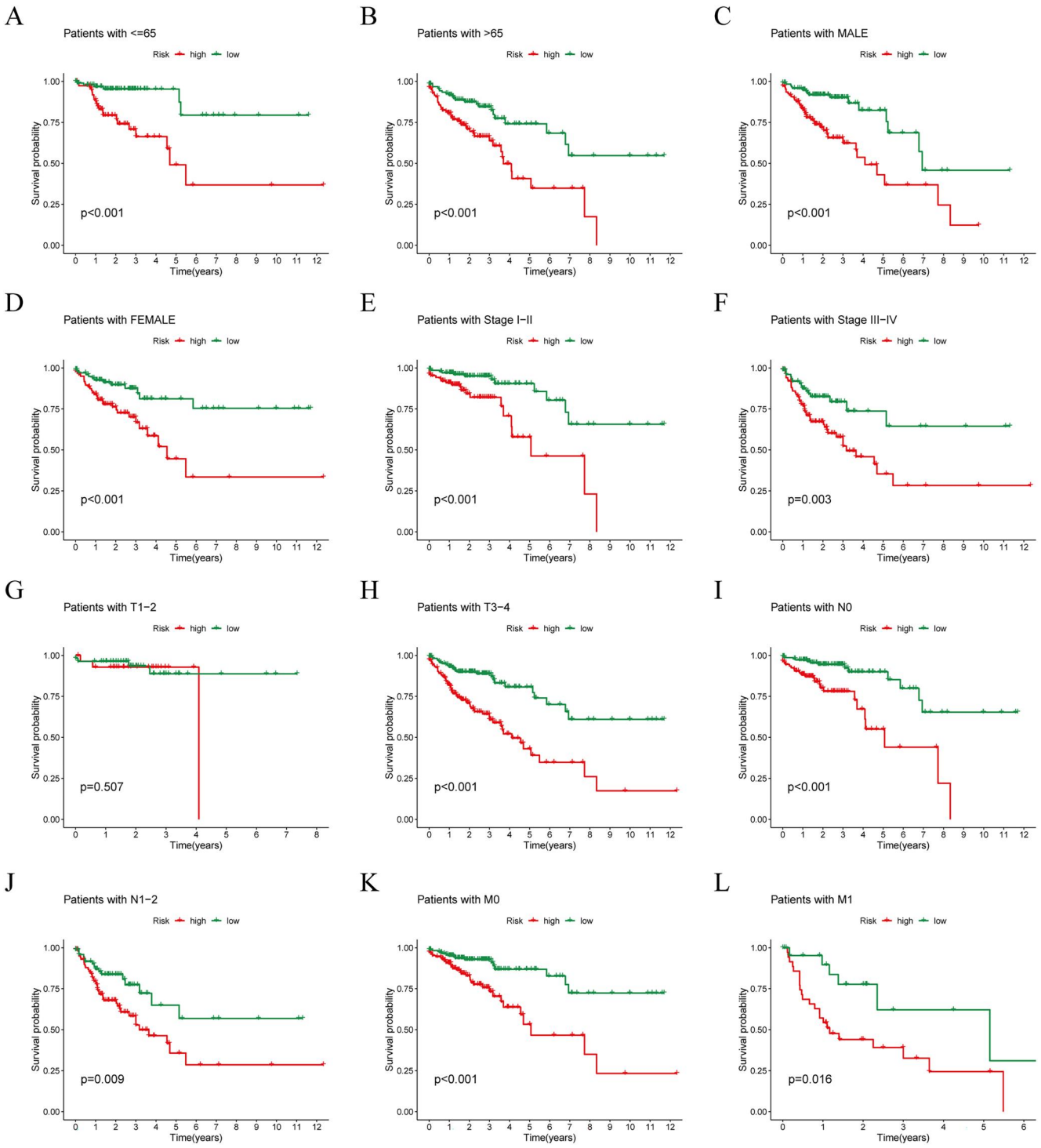


**FIGURE 4** Kaplan–Meier analysis of survival probabilities for various clinical variables. (a–l) The survival probabilities for various clinical variables in the high-risk group were lower than in the low-risk group in all subgroups except for patients in the T1-2 subgroup.

patients in the high-risk group had significantly worse survival probabilities due to the M2 macrophage phenotype (Figures 7b,c). In order to further investigate the differences between low- and high-risk groups, the comparison of ssGSEA scores was conducted using ssGSEA analysis. The results indicated that immature dendritic cells, mast cells, T helper 2 cells (Th2 cells), and regulatory T cells (Treg cells) were associated with the low-risk group (Figure 7d). Moreover, an evaluation of the immune function was conducted to explore potential immune pathways involved in distinguishing between patients at different risk levels. Our observations demonstrated that adenomatous polyposis coli (APC) co (Antigen-presenting cell) stimulation, CCR (chemokine receptor), major histocompatibility complex class I and para-inflammation were more active in the low-risk group (Figure 7e). Additionally, considering the significance of immune checkpoints in immunotherapy, we assessed the expression of immune checkpoints in both the high-risk and

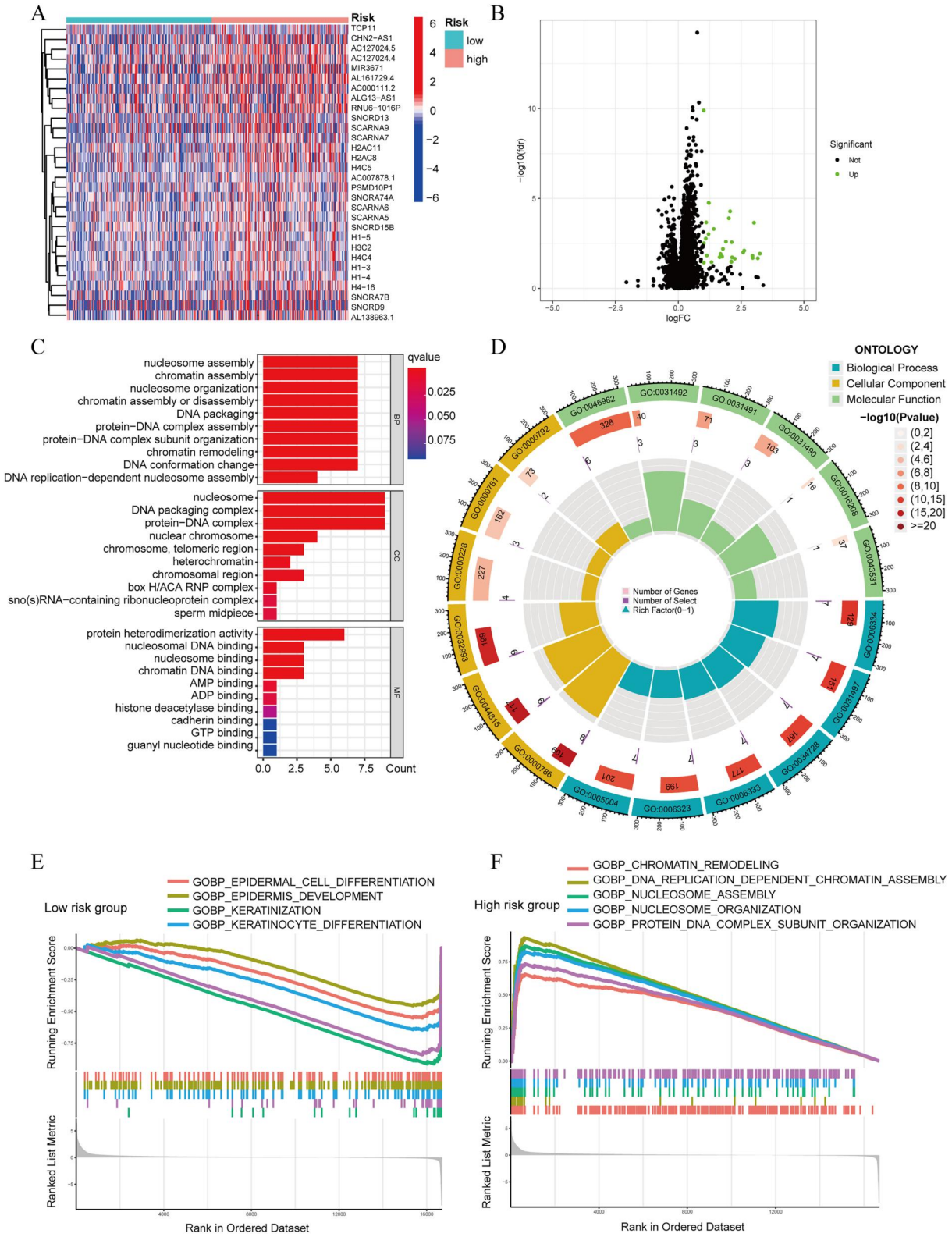


**FIGURE 5** Identification of DEGs and Functional enrichment analysis in low- and high-risk groups. (a) The heatmap showed the top 30 significant genes of DEGs. (b) The volcano plots of DEGs with green for upregulated genes and black for downregulated genes. (c,d) The top enriched Gene ontology (GO) terms in biological process (BP), cellular component (CC) and molecular function (MF). (e,f) GO GSEA enrichment analysis of DEGs between the low- and high-risk groups. DEGs, differentially expressed genes; GSEA, gene set enrichment analysis.

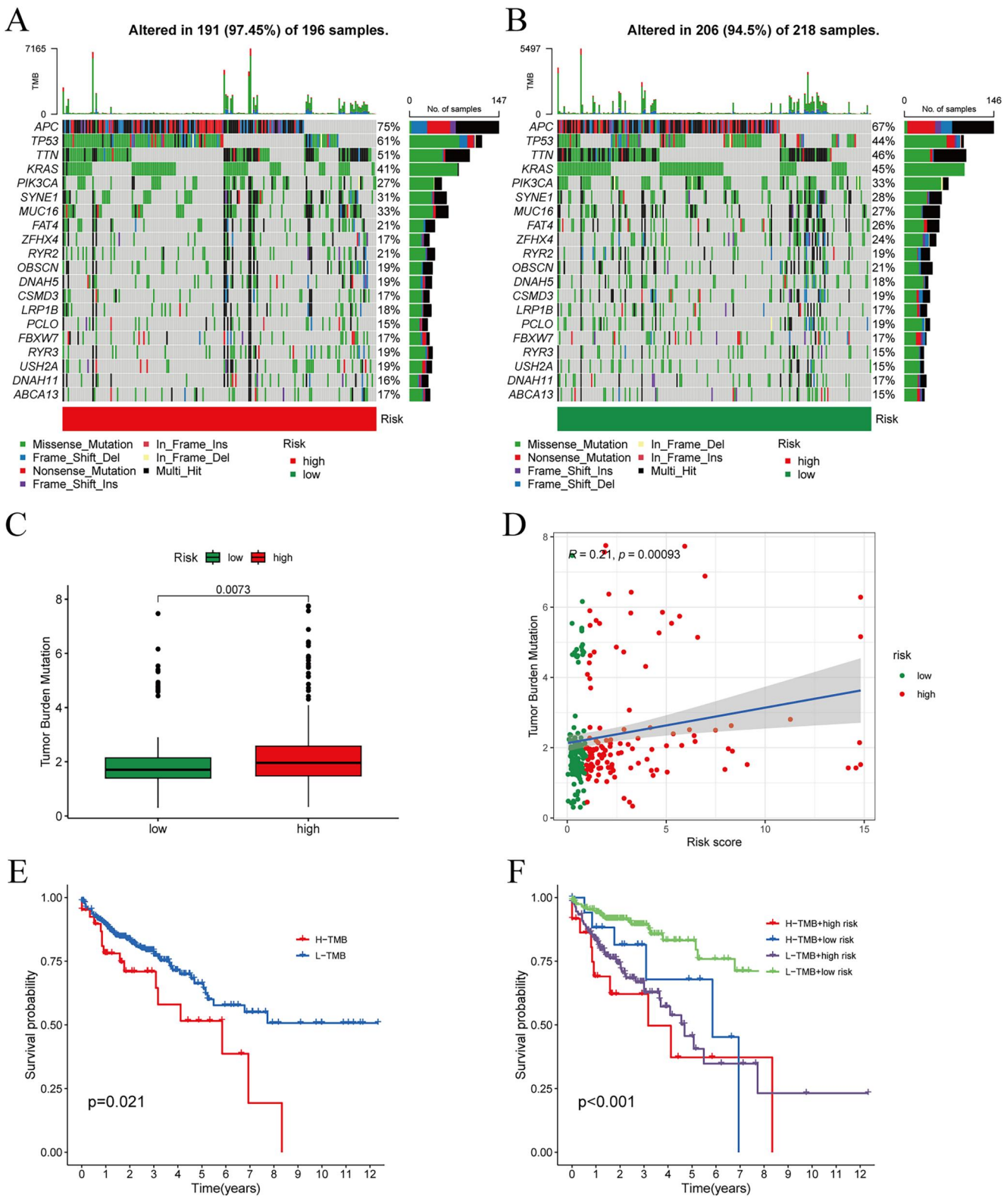


**FIGURE 6** The relationship of the prognostic model with tumour somatic mutation and TMB. (a,b) The waterfall plot of tumour somatic mutation in low- and high-risk groups. (c,d) Different TMB levels in low-and high-risk groups. (e) Survival status of low TMB levels and high TMB levels in patients with CCOAD. (f) The Kaplan–Meier curves of OS in different groups of TMB combination with risk scores. COAD, Colon adenocarcinoma; OS, overall survival; TMB, tumour mutational burden.

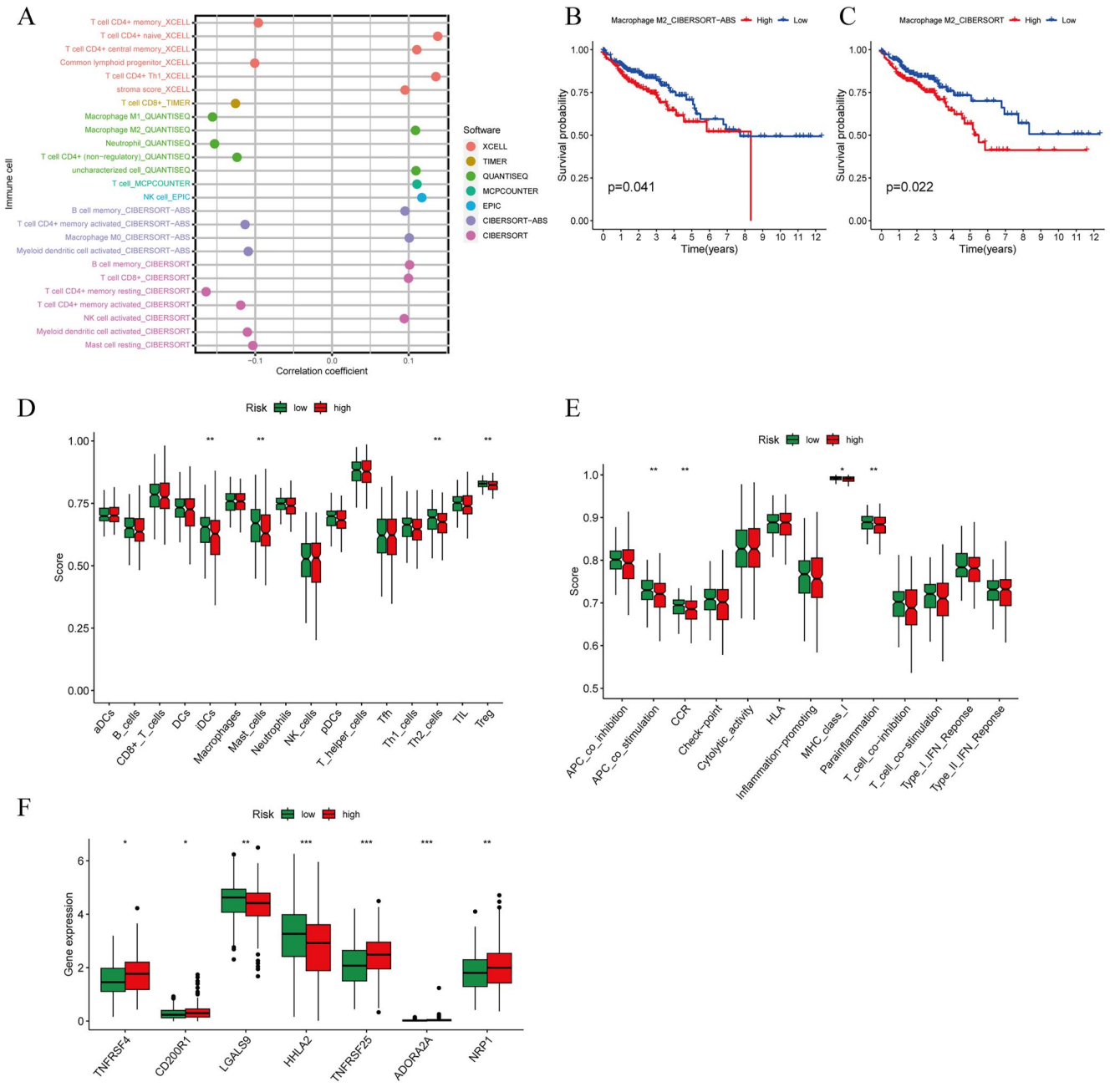


**FIGURE 7** The immune cell infiltration and function analysis between the low- and high-risk groups. (a) The correlation coefficient of immune cells in 7 software. (b,c) The survival probability of macrophages M2 between the low- and high-risk groups in CIBERSORT-ABS and CIBERSORT. (d) The boxplots described the cores of 16 immune cells. (e) The boxplots showed the cores of 13 immune-related functions. (f) The boxplots of seven immune checkpoints in the entire cohort. (***$p < 0.001$, **$p < 0.01$, *$p < 0.05$).

low-risk groups. As depicted in Figure 7f, TNFRSF4, CD200R1, TNFRSF25, ADORA2A, and NRP1 were highly expressed in the high-risk group, while LGALS9 and HHLA2 exhibited increased expression in the low-risk group.

## 3.8 | Chemotherapeutic drug sensitivity analysis

Tumour drug sensitivity analysis was conducted using the pRRophetic R package. The IC50 values of 13 commonly utilised chemotherapeutic drugs for colorectal cancer were studied in both the low- and high-risk groups. Significantly distinct IC50 values were observed for these agents (Alpelisib, Dasatinib, IGF1R3801, Ipatasertib, Linsitinib, Taselisib, MK-1775, Nilotinib, Pictilisib, PRIMA-1MET, Sepantronium bromide, and Vorinostat) between the two groups. Notably, the IC50 values of these drugs were higher in the low-risk group compared to the high-risk group, suggesting that patients in the high-risk group exhibited greater sensitivity to chemotherapeutic drugs (Figures 8a–l).

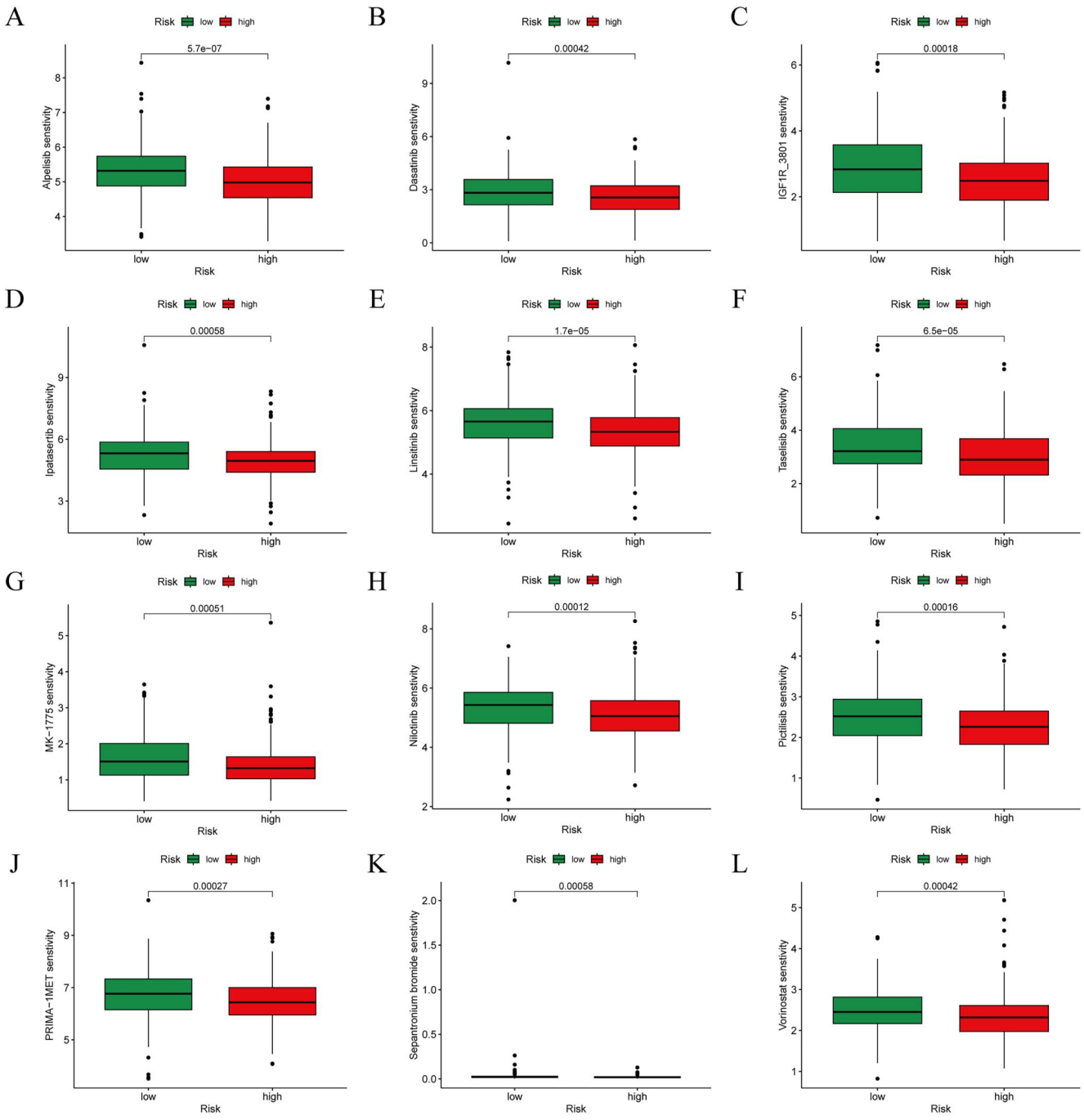


**FIGURE 8** Analysis of chemotherapeutic agent sensitivity. (a–l) The IC50 values of chemotherapeutic agents (Alpelisib, Dasatinib, IGF1R3801, Ipatasertib, Linsitinib, Taselisib, MK-1775, Nilotinib, Pictilisib, PRIMA-1MET, Sepantronium bromide, and Vorinostat) between the high- and low-risk groups.

## 3.9 | Association of consensus clustering of 8 prognostic lncRNAs with characteristics, OS and immune analysis of COAD patients

Unsupervised consensus clustering was employed to identify potential distinct COAD clusters based on the 8 prognostic lncRNAs. By evaluating the mean silhouette score, we analysed clusters with $k < 10$ and determined that the optimal clustering solution was $k = 2$ (Figure 9a–d). Subsequently, all COAD patients were divided into Cluster 1 ($n = 227$) and Cluster 2 ($n = 219$). As depicted in Figure 9e, patients in Cluster one exhibited significantly worse survival probabilities compared to those in Cluster 2. To further elucidate the contribution of each cluster type to the two groups, a Sankey diagram was utilised. The analysis revealed that Cluster 2 predominantly belonged to the low-risk group, while Cluster 1 predominantly belonged to the high-risk group (Figure 10a). Additionally, PCA and t-SNE results demonstrated distinct distribution

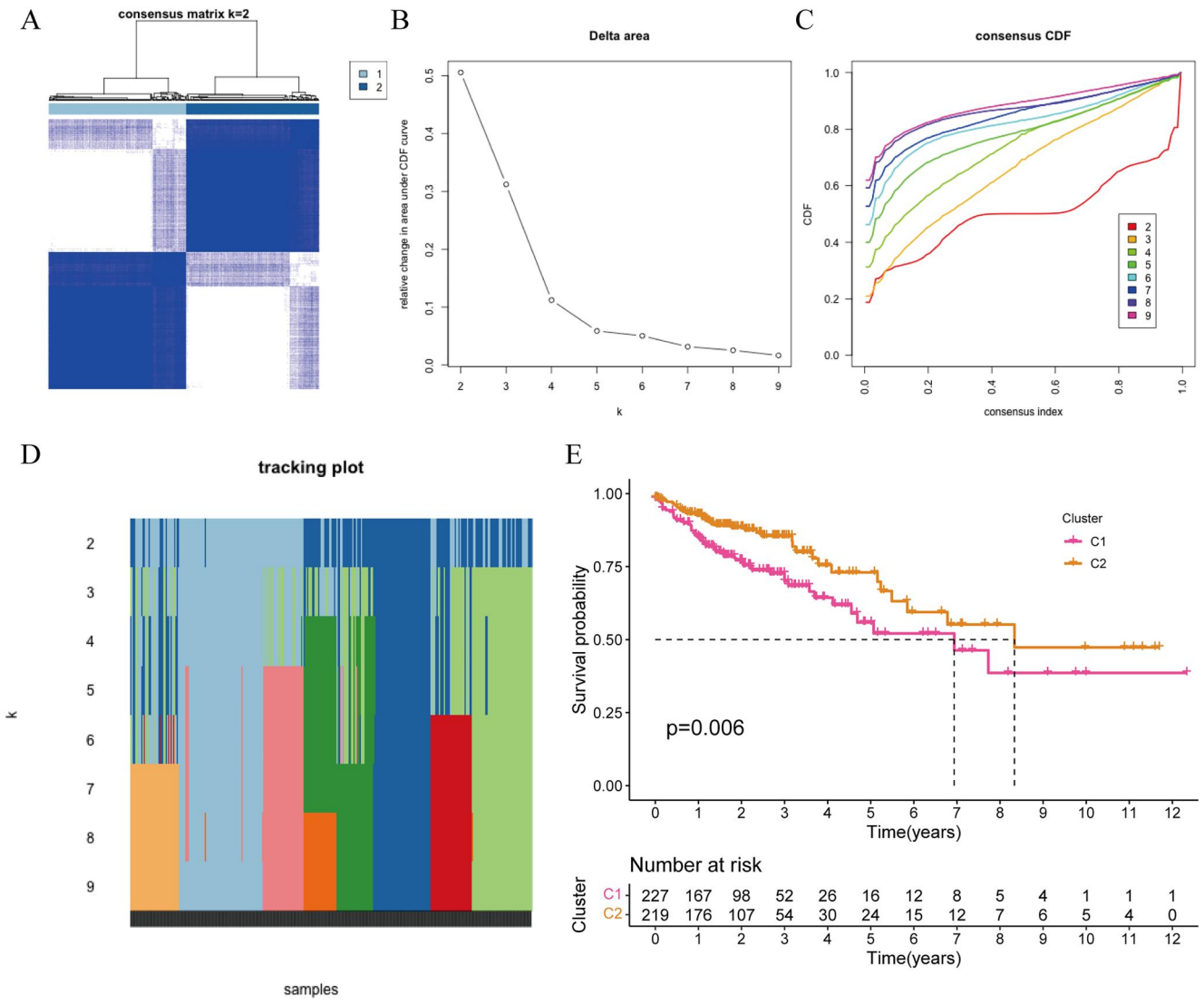


**FIGURE 9** Unsupervised consensus clustering of disulfidptosis-related lncRNAs. (a) The heatmap of the consensus matrix ($k = 2$). (b) Consensus clustering cumulative distribution function (CDF). (c) The relative changing area under the CDF curve (d) The tracking plot of k from 2 to 9. (e) The Kaplan–Meier curves of OS in different clusters. OS, overall survival.

patterns of patients in different risk and clustering groups, consistent with the trends observed in the Sankey diagram (Figures 10b–e). Immune infiltration patterns based on cluster classification were depicted in a heatmap using TIMER, CIBERSORT, CIBERSORT-ABS, QUANTISEQ, MCPCOUNTER, XCELL, and EPIC algorithms (Figure 10f). Furthermore, we explored immune cell infiltration and the expression of immune checkpoints in different clusters, comparing them with the high-risk and low-risk groups. The results indicated that the expression trends of immune checkpoints aligned with the aforementioned data (Figure 7f, 10g). Subsequently, significant differences in IC50 values of chemotherapeutic drugs (Alpelisib, IGF1R3801, Vorinostat, Linsitinib, MK-1775, Nilotinib, Pictilisib, PRIMA-1MET, and Taselisib) were found between Cluster 1 and Cluster 2. These findings reinforced the observation that patients in Cluster 1 exhibited greater sensitivity to chemotherapeutic drugs, consistent with the previous results (Figures 8a–m, Figures S2a–i).

## 3.10 | Establishment of a prognostic nomogram

We integrated age, stage, metastasis, and risk score to construct a comprehensive nomogram for predicting patients' prognoses at 1-, 2-, and 3-year (Figure 10h). When the cumulative score for a patient reaches 104, their 1-, 2-, and 3-year survival rates are 0.99, 0.983, and 0.977, respectively, indicating a favourable prognosis. We also generated calibration curves, and for the 1-, 2-, and 3-year timeframes, the curves closely aligned with the diagonal line, revealing a favourable correspondence with actual observations (Figure 10i).

## 3.11 | In vitro validation of prognostic lncRNAs expression and chemosensitivity

After conducting bioinformatics analyses, we proceeded with in vitro experimental verification. NCM460 and HCT116 cell

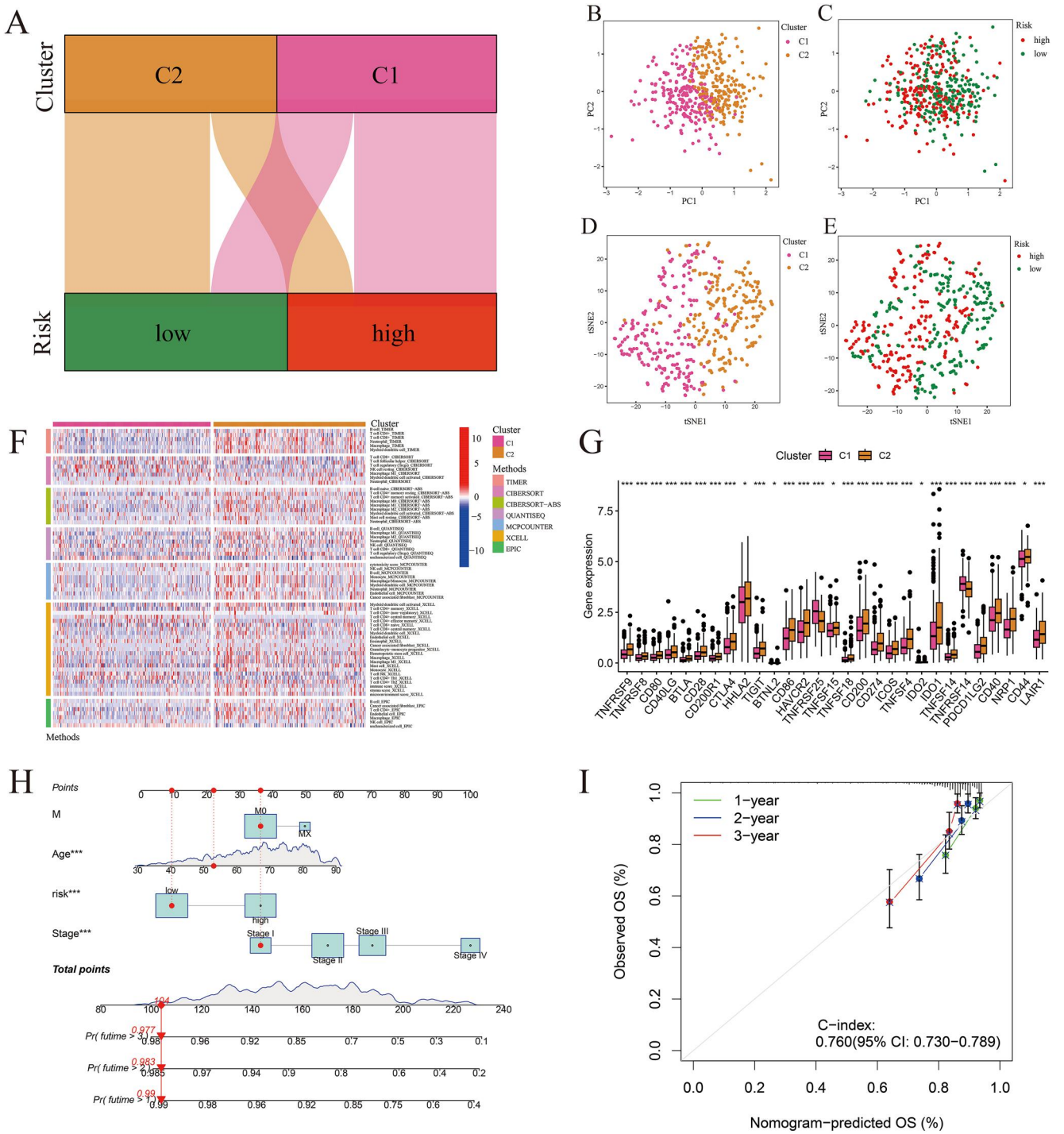


**FIGURE 10** Assessment of disulfidptosis-related cluster and immune cell infiltration characteristics analysis. (a) Sankey diagram of association between classifications. (b) The Principal Component Analysis (PCA) score plot of cluster 1 and 2. (c) The PCA score plot of low-risk and high-risk groups. (d) T-SNE plot of cluster 1 and 2. (e) T-SNE plot of low-risk and high-risk groups. (f) The heatmap of immune cells in 7 software between the two clusters. (g) The boxplots of 29 immune checkpoints between the two clusters. (h) Establishment of a nomogram based on age, stage, metastasis, and risk scores. (i) The calibration curve for nomogram at 1, 2, and 3 years (***$p < 0.001$, **$p < 0.01$, *$p < 0.05$). PCA, principal component analysis.

lines were utilised to represent human normal colon cells and colorectal cancer cells, respectively. The expression levels of eight lncRNAs (FENDRR, SNHG7, AP003555.1, AL513550.1, AL138756.1, LINC01235, AC002091.2, ATP2-A1-AS1) were assessed through qRT-PCR. Figure 11a demonstrated a significant decrease in FENDRR expression in HCT116 cells compared to NCM460 cells. Additionally, the expression levels of the other five lncRNAs in HCT116 cells were higher than those in NCM460 cells (Figures 11b–f). Furthermore, although not statistically significant, AC002091.2

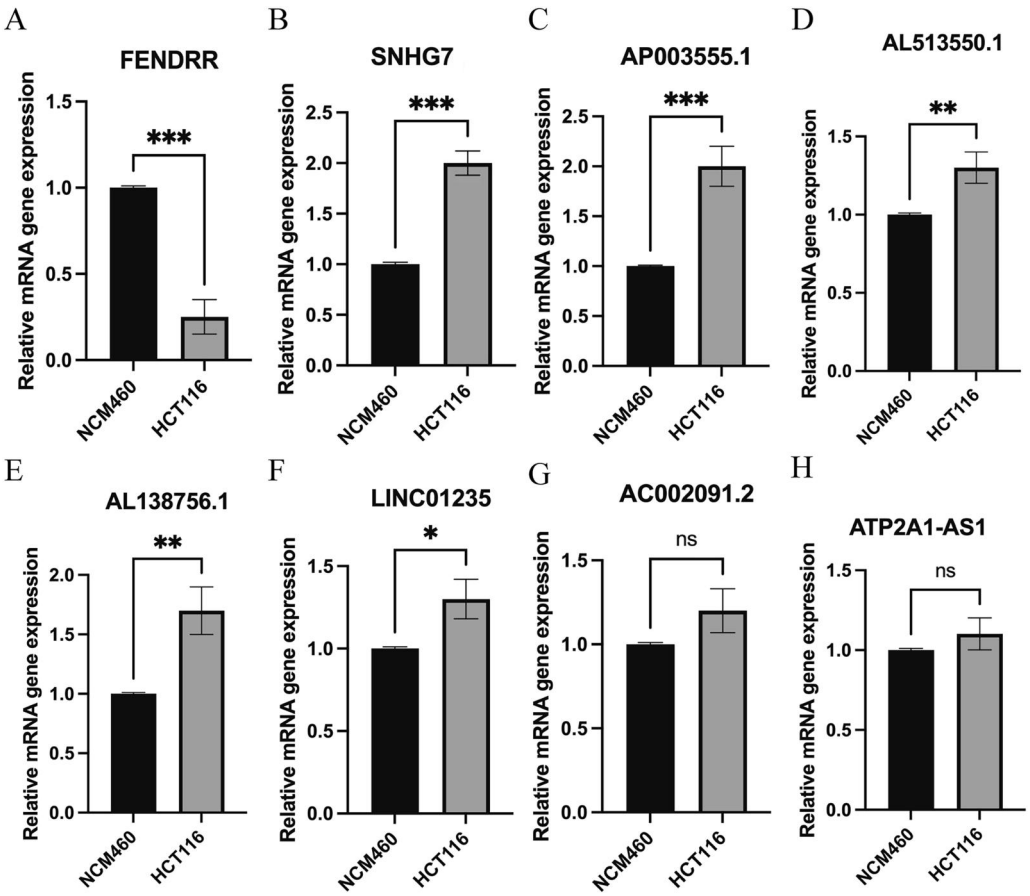


**FIGURE 11** Validation of 8 prognostic lncRNAs by Quantitative real-time PCR (qRT-PCR) in vitro. (a–h) The expression levels of lncRNAs in NCM460 and HCT116 cells. (***$p < 0.001$, **$p < 0.01$, *$p < 0.05$, ns = no significance). qRT-PCR, quantitative real-time PCR.

and ATP2A1-AS1 also exhibited an inclination towards upregulation (Figures 11g,h).

### 3.12 | The lncRNAs participated in mediating the proliferation and migration of COAD cells

In order to investigate the potential role of lncRNAs in COAD, we conducted in vitro experiments. Based on the expression levels of lncRNAs in HCT116 cells, we performed overexpression or knockdown experiments for the top three lncRNAs (FENDRR, SNHG7, and AP003555.1) to examine their impact on cell proliferation and migration. The efficiency of overexpression or knockdown was confirmed through RT-qPCR analysis (Figure 12a). Our findings revealed that the knockdown of AP003555.1 did not significantly affect COAD cell viability. However, both the overexpression of FENDRR and the knockdown of SNHG7 inhibited the growth of HCT116 cells (Figure 12b). Additionally, cell scratch assays were employed to evaluate the influence of FENDRR and SNHG7 on cell migration. As depicted in Figures 12c,d, overexpression or knockdown resulted in a significant reduction in the migration ability of HCT116 cells. Furthermore, the colony formation assay confirmed that overexpression of FENDRR or knockdown of SNHG7 suppressed the proliferation of HCT116 cells (Figures 12e,f). In conclusion, our results suggest that the expression of lncRNAs FENDRR and SNHG7 affected the proliferation and migration of HCT116 cells. These lncRNAs may serve as key factors in addressing the unsatisfactory therapeutic outcomes observed in COAD patients.

## 4 | DISCUSSION

In recent years, several forms of regulated cell death have emerged, including apoptosis, pyroptosis, necroptosis, and ferroptosis [16, 17]. Disulfidptosis and cuproptosis are two forms of programmed cell death that are closely associated with glycolysis, a crucial metabolic pathway in tumour cells. Studies have shown that products of glycolysis can regulate the activity of disulfidptosis and cuproptosis pathways, thus impacting the fate of tumour cells [11, 13, 18]. These findings identify the significant role of glycolysis in tumour cell metabolism, underscoring the importance of investigating the interplay between disulfidptosis and cuproptosis for a better understanding of the molecular mechanisms underlying tumour cell metabolism and programmed cell death processes.

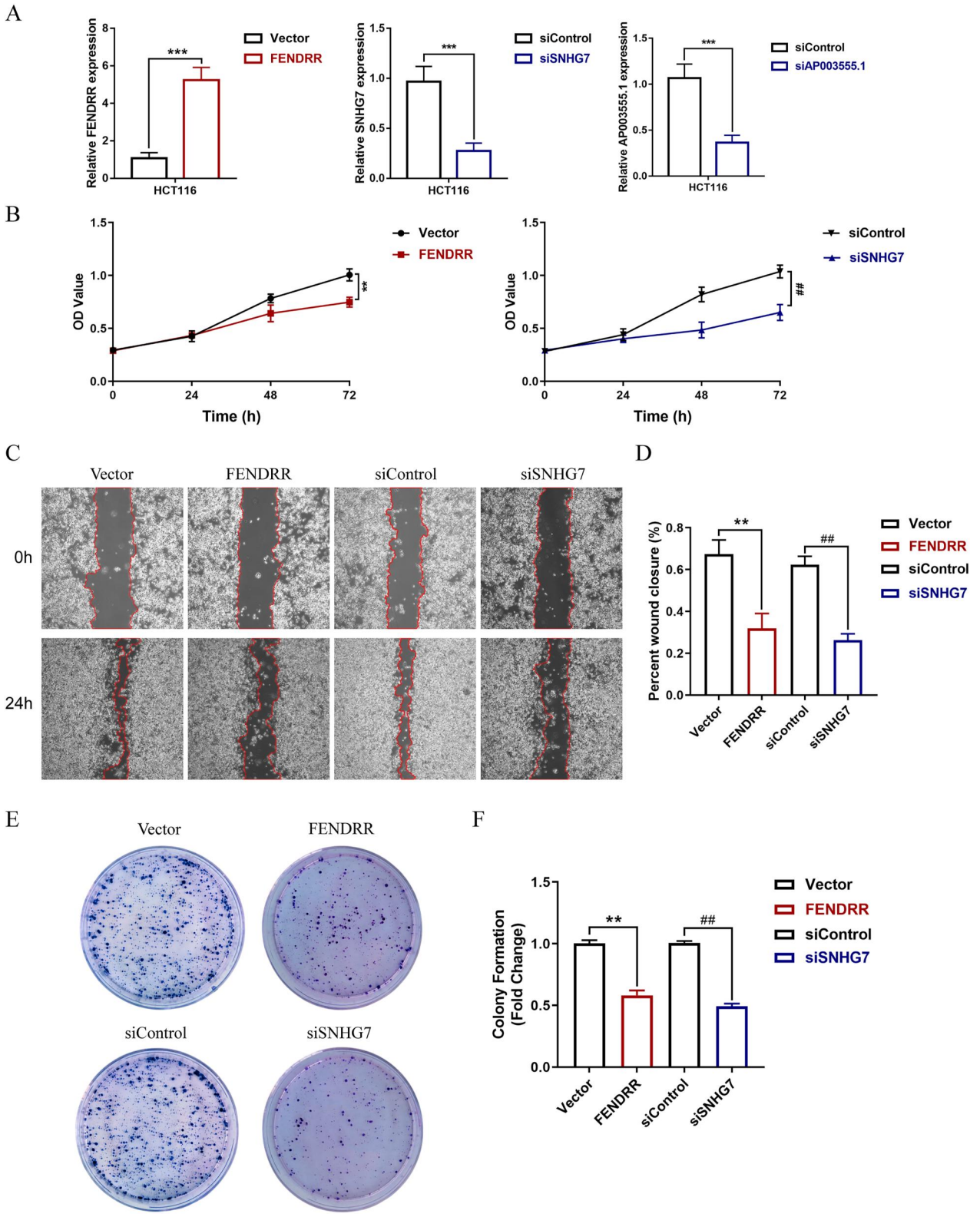


**FIGURE 12** FENDRR and SNHG7 mediated HCT116 cells proliferation and migration in vitro. (a) The expression levels of FENDRR, SNHG7, and AP003555.1 were analysed by qRT-PCR. (b) Growth curves of HCT116 cells, overexpressing FENDRR, and siSNHG7 were determined via CCK-8 assays. (c,d) Overexpressing FENDRR and siSNHG7 resulted in a slower cellular migration rate by wound-healing assays. (e,f) Colony formation assays showed that overexpressing FENDRR and siSNHG7 inhibited HCT116 cells proliferation, respectively. qRT-PCR, quantitative real-time PCR. (***$p < 0.001$, **$p < 0.01$, *$p < 0.05$, ns = no significance).

In this study, we developed a prognostic model that utilises disulfidptosis- and cuproptosis-related lncRNAs to predict the prognosis and sensitivity to chemotherapeutic drugs in COAD patients. Additionally, we performed functional enrichment analysis, evaluated the TMB, and assessed the infiltration of tumour immune cells to investigate the underlying molecular mechanisms. Furthermore, we identified a disulfidptosis- and cuproptosis-related cluster that exhibited strong associations with immune cell infiltration and chemosensitivity. The lncRNA prognostic model has the potential to contribute to our understanding of clinical-pathological characteristics, mechanisms of chemotherapy response, and serve as reliable biomarkers for distinguishing between "cold tumours" and "hot tumours," as well as predicting the efficacy of chemotherapeutic drugs in COAD patients.

Growing evidence suggests that the expression of lncRNAs plays a crucial role in the oncogenic processes of COAD. In this study, we identified 1309 lncRNAs and developed a novel prognostic model comprising 8 lncRNAs for COAD. By utilising the expression levels of these 8 lncRNAs and calculating the corresponding risk scores, we successfully stratified patients into low- and high-risk groups in both the TCGA dataset and the training and testing cohorts. The survival analysis of the lncRNAs prognostic model accurately predicted the OS of COAD patients across all cohorts. Notably, the AUC of clinical characteristics indicated that the risk scores derived from this model exhibited a superior predictive value. Additionally, the time-dependent ROC curves demonstrated AUCs of 0.764, 0.740, and 0.686 at 1-, 3-, and 5-year time points, respectively, in the TCGA dataset, suggesting that the model possessed robust predictive capabilities for patient survival. In conclusion, we have successfully developed and validated a novel prognostic model related to disulfidptosis and cuproptosis for predicting the prognosis of COAD patients.

The aberrant expression of lncRNAs holds significant promise in the early detection, treatment response monitoring, and prognosis of cancer [19]. In our study, we successfully identified 8 lncRNAs (FENDRR, SNHG7, AP003555.1, AL513550.1, AL138756.1, LINC01235, AC002091.2, and ATP2A1-AS1). Subsequent in vitro experiments confirmed the differential expression of these lncRNAs in HCT-116 cells compared to human normal colon cells. Previous studies have shed light on the biological functions of several of these lncRNAs. For example, SNHG7 has been shown to enhance the invasiveness and migratory abilities of gastric cancer cells by inhibiting the miR-34a-Snail-EMT axis [20]. FENDRR, on the other hand, has demonstrated associations with various clinical characteristics in different cancers and has exhibited potential as a novel diagnostic and prognostic biomarker [21, 22]. Further evidence suggests that FENDRR acts as a miRNA sponge for miR-214-3p, thereby suppressing the progression of gastric cancer [23]. Moreover, AL513550.1 has been implicated in elucidating the link between survival prognosis and N7-methylguanosine modification-related lncRNAs in oral squamous cell carcinoma [24]. Similarly, ATP2A1-AS1 has emerged as a promising prognostic biomarker for patients with cervical cancer [25]. Additionally, LINC01235 and AL138756.1 have been identified as predictors of clinical features and prognosis in stomach adenocarcinoma and colorectal cancer, respectively [26–28]. Based on the aforementioned research, these lncRNAs exert crucial biological functions and participate in the regulation of cancer progression, thereby furnishing the molecular groundwork for the development of a disulfidptosis- and cuproptosis-related lncRNA prognostic model.

Moreover, we conducted a comprehensive investigation to explore the potential signalling pathways involved in mediating disulfidptosis and cuproptosis using GO and GSEA enrichment analyses. The GO analysis revealed that DEGs between low-risk and high-risk patient groups were enriched in pathways such as nucleosome assembly, chromatin assembly, nucleosome organisation, and DNA packaging. Notably, the GSEA analysis demonstrated a significant enrichment of similar signalling pathways, including chromatin remodelling, DNA replication-dependent chromatin assembly, nucleosome assembly, nucleosome organisation, and protein DNA complex subunit organisation, in the high-risk group. Mounting evidence suggests that alterations in nucleosomes contribute to various diseases, including infections, inflammation, benign conditions, and malignant tumours [29]. Mutations or modifications in factors involved in nucleosome assembly have been associated with cancer development [30]. Additionally, nucleosome remodelling plays a crucial role in chromatin assembly and reorganisation, which holds significant implications for cancer progression [31]. A previous study indicated that H3K56 acetylation is involved in chromatin assembly and DNA repair, exerting a significant effect on malignancies [32]. These findings confirmed that the expression of the 8 disulfidptosis- and cuproptosis-related lncRNAs contributes to tumourigenesis and disease progression through the aforementioned signalling pathways. Considering the association between these signalling pathways and lncRNAs, further investigations are warranted to elucidate the specific molecular mechanisms underlying disulfidptosis and cuproptosis in patients with COAD.

TMB has emerged as a potential biomarker for predicting the efficacy of immunotherapy across multiple types of human cancer [33]. In this study, we identified the top 20 mutated genes in both low- and high-risk groups, observing a higher frequency of gene mutations in the high-risk group. Notably, adenomatous polyposis coli (APC), tumour protein p53 (TP53), and titin (TTN) were found to be the most commonly mutated genes, with a mutation rate exceeding 50% in the high-risk group. APC holds the distinction of being the most frequently mutated gene in human malignancies. Mutations in the tumour suppressor gene APC are closely associated with over 80% of sporadic colorectal cancers through an aberrant activation of the Wnt signalling pathway [34]. Moreover, previous research has implicated mutant p53 in the maintenance of inflammation in colorectal cancer, which is known to drive tumour progression [35]. Furthermore, our findings revealed that patients with high TMB in the high- or low-risk group exhibited a poorer probability of survival compared to those with low TMB. TMB was shown to be prognostic for patients

with COAD, as smoking and high TMB contribute to the generation of immunogenic neoantigens in non-small cell lung cancer [36]. Consequently, high TMB led to high tumour neoantigen burden, which was more effective for checkpoint blocking immunotherapy [37]. Importantly, several clinical studies have reported notably higher clinical benefit rates among patients with high TMB who received immune checkpoint inhibitor therapy [38, 39]. Thus, TMB represents a promising biomarker for predicting the response to immunotherapy in patients with COAD.

In recent years, due to the growing understanding of tumour immunobiology and the development of immunotherapeutic agents, immunotherapy has emerged as a highly valuable clinical approach [40]. Based on the immune cell infiltration in the tumour microenvironment, tumours can be categorised into two types: 'cold tumours' and 'hot tumours'. 'Cold tumours' are characterised by a lack of immune cells and an immune-desert phenotype, rendering them unresponsive to immunotherapy. On the other hand, 'hot tumours' exhibit abundant immune cell infiltration and a hyperactive immune response, making them more responsive to immunotherapy [41]. In our study, we observed a significant increase in the infiltration levels of T cells, macrophages, B cells, NK cells, and mast cells in high-risk patients. Furthermore, high expression of immune checkpoint markers, including TNFRSF4, CD200R1, TNFRSF25, ADORA2A, and NRP1, was also detected in the high-risk group. Importantly, it is worth noting that the efficacy of immunotherapy is influenced by the tumour microenvironment, as demonstrated in various studies [42]. Previous research has highlighted the heterogeneous outcomes of immunotherapy in colorectal cancer patients with different tumour microenvironments [43]. Therefore, comprehensive investigations are warranted to elucidate the roles of disulfitopsis- and cuproptosis-related lncRNAs in the tumour microenvironment and its impact on immunotherapy.

It is widely recognised that COAD exhibits resistance to various chemotherapeutic agents, both in monotherapy and combination therapy settings [44]. The development of chemoresistance in COAD poses a significant challenge to effective treatment, leading to disease progression and reduced survival outcomes [45]. However, our study conducted a chemotherapeutic drug sensitivity analysis and revealed that patients in the high-risk group exhibited lower IC50 values for multiple anti-tumour drugs. This finding suggests the potential for designing more targeted treatment schedules for COAD. Consequently, it is crucial to establish appropriate chemotherapy regimens tailored to patients in different risk groups.

Based on the 8 prognostic lncRNAs, consensus clustering analysis was conducted to identify distinct COAD clusters. This approach aimed to further validate the differences between risk-based divisions and the findings from bioinformatic and immune-related analyses. In our present study, we observed that patients from different risk groups and clusters were predominantly distributed along two trajectories, with C1 exhibiting predominantly high values and C2 predominantly low values. The patterns of immune infiltration and immune checkpoint expression in different clusters were consistent with those observed in different risk groups. Furthermore, cluster 1 displayed lower IC50 values for chemotherapy drugs, indicating a higher sensitivity to chemotherapy, which mirrored the characteristics of patients in the high-risk group. To further establish the reliability of the prognostic model incorporating these lncRNAs, we assessed the expression levels of these 8 disulfidptosis-related lncRNAs in different cell lines (NCM460 and HCT116 cells) using qRT-PCR. Our findings were consistent with the TCGA dataset. Notably, five lncRNAs exhibited significantly higher expression levels in HCT116 cells compared to normal colon epithelial cells, while FENDRR expression in HCT116 cells was notably reduced. It is worth mentioning that FENDRR acts as a tumour suppressor by functioning as a miRNA sponge.

Accumulating evidence supports the implication of lncRNAs, specifically FENDRR and SNHG7, in the development and progression of COAD. FENDRR functions as a tumour suppressor [46], whereas SNHG7 promotes tumour growth and invasion. Notably, SNHG7 is involved in regulating tumour glycolysis and affects tumour progression. High expression of SNHG7 was observed in prostate cancer (PCa) tissues and cells, and its silencing resulted in suppressed proliferation and glycolysis in PCa cells [47]. In gastric cancer, SNHG7 is significantly upregulated and associated with cisplatin resistance. Silencing SNHG7 enhances sensitivity to cisplatin and promotes glycolysis in gastric cancer cells by targeting LDHA, a glycolysis enzyme, revealing a regulatory mechanism for SNHG7-mediated cisplatin resistance [48]. Furthermore, SNHG7 is overexpressed in early-stage colon cancer and colon advanced adenomas, and its downregulation suppresses cell proliferation by inhibiting the K-ras/ERK/cyclin D1 signalling pathway [49]. Consistent with these observations, our in vitro findings substantiate the importance of FENDRR and SNHG7 in the pathology of COAD. Importantly, our study demonstrates a close association between FENDRR and SNHG7 with disulfidptosis and cuproptosis in COAD patients. Taken together, it is speculated that these lncRNAs may play a pivotal role in regulating the proliferation and migration of colorectal cancer cells through specific molecular mechanisms, possibly involving tumour cell metabolism. Consequently, tumour cell metabolism, particularly glycolysis, may serve as a crucial mediator and bridge in the regulation of cellular programmed cell death, such as disulfidptosis and cuproptosis. While further research is needed to fully elucidate the precise mechanisms by which these lncRNAs regulate disulfidptosis and cuproptosis, our study provides valuable insights for identifying new therapeutic targets in patients with COAD.

## 5 | CONCLUSION

In summary, our study has successfully developed a novel prognostic model and cluster associated with disulfidptosis and cuproptosis, comprising 8 lncRNAs. The model and cluster demonstrated a significant value in prognostic prediction, immune cell infiltration, and chemosensitivity among COAD

patients. Moreover, we observed that the disulfidptosis- and cuproptosis-related lncRNAs FENDRR and SNHG7 have a direct impact on the proliferation and migration of HCT116 cells, which may provide new insights into understanding the complex interplay between tumour cell metabolism and programmed cell death processes.

## AUTHOR CONTRIBUTIONS

Qiang Fan and Guang-Bo Wu: Writing – original draft. Lei Zheng and Hong-Jie Li: Writing – reviewing and editing. Min Chen: Data curation. Lv-Zhu Xiang: Methodology. Lv-Zhu Xiang: Supervision. Meng Luo: Funding acquisition. All authors read and approved the final manuscript.

## ACKNOWLEDGEMENTS

This work was supported by The National Natural Science Foundation of China (No. 81970526, 81900550, 82100639, 82200630). The Clinical Research Programme of 9th People's Hospital, Shanghai Jiao Tong University School of Medicine (JYLJ202124) and Fundamental research programme funding of Ninth People's Hospital affiliated to Shanghai Jiao Tong University School of Medicine (JYZZ162).

## CONFLICT OF INTEREST STATEMENT

The authors declare that they have no known competing financial interests or personal relationships that could have appeared to influence the work reported in this paper.

## DATA AVAILABILITY STATEMENT

The data sets supporting the results of this article are included within the article and its additional files.

## ETHICS APPROVAL AND CONSENT TO PARTICIPATE

Not applicable.

## CONSENT FOR PUBLICATION

All authors know and agree to publish the article.

## ORCID

*Meng Luo* https://orcid.org/0000-0003-3975-7476

## REFERENCES

1. Zhou, X.G., et al.: Identifying miRNA and gene modules of colon cancer associated with pathological stage by weighted gene co-expression network analysis. OncoTargets Ther. 11, 2815–2830 (2018). https://doi.org/10.2147/ott.s163891
2. Wu, M., et al.: Integrated analysis of distant metastasis-associated genes and potential drugs in colon adenocarcinoma. Front. Oncol. 10, 576615 (2020). https://doi.org/10.3389/fonc.2020.576615
3. Wolf, A.M.D., et al.: Colorectal cancer screening for average-risk adults: 2018 guideline update from the American Cancer Society. CA Cancer J. Clin. 68(4), 250–281 (2018). https://doi.org/10.3322/caac.21457
4. Brahmer, J.R., et al.: Management of immune-related adverse events in patients treated with immune checkpoint inhibitor therapy: American society of clinical oncology clinical practice guideline. J. Clin. Oncol. 36(17), 1714–1768 (2018). https://doi.org/10.1200/jco.2017.77.6385
5. Prizment, A.E., et al.: Tumor eosinophil infiltration and improved survival of colorectal cancer patients: Iowa Women's Health Study. Mod. Pathol. 29(5), 516–527 (2016). https://doi.org/10.1038/modpathol.2016.42
6. Liu, X., et al.: Actin cytoskeleton vulnerability to disulfide stress mediates disulfidptosis. Nat. Cell Biol. 25(3), 404–414 (2023). https://doi.org/10.1038/s41556-023-01091-2
7. Bhutia, Y.D., et al.: Amino Acid transporters in cancer and their relevance to "glutamine addiction": novel targets for the design of a new class of anticancer drugs. Cancer Res. 75(9), 1782–1788 (2015). https://doi.org/10.1158/0008-5472.can-14-3745
8. Lo, M., Wang, Y.Z., Gout, P.W.: The x(c)- cystine/glutamate antiporter: a potential target for therapy of cancer and other diseases. J. Cell. Physiol. 215(3), 593–602 (2008). https://doi.org/10.1002/jcp.21366
9. Koppula, P., et al.: Amino acid transporter SLC7A11/xCT at the crossroads of regulating redox homeostasis and nutrient dependency of cancer. Cancer Commun. 38(1), 12–13 (2018). https://doi.org/10.1186/s40880-018-0288-x
10. Liu, X., et al.: Cystine transporter regulation of pentose phosphate pathway dependency and disulfide stress exposes a targetable metabolic vulnerability in cancer. Nat. Cell Biol. 22(4), 476–486 (2020). https://doi.org/10.1038/s41556-020-0496-x
11. Wang, Z., et al.: Based on disulfidptosis-related glycolytic genes to construct a signature for predicting prognosis and immune infiltration analysis of hepatocellular carcinoma. Front. Immunol. 14, 1204338 (2023). https://doi.org/10.3389/fimmu.2023.1204338
12. Xu, M., et al.: Construction and validation of a cuproptosis-related lncRNA signature as a novel and robust prognostic model for colon adenocarcinoma. Front. Oncol. 12, 961213 (2022). https://doi.org/10.3389/fonc.2022.961213
13. Yang, W., et al.: 4-Octyl itaconate inhibits aerobic glycolysis by targeting GAPDH to promote cuproptosis in colorectal cancer. Biomed. Pharmacother. 159, 114301 (2023). https://doi.org/10.1016/j.biopha.2023.114301
14. Li, J., Yang, C., Zheng, Y.: A novel disulfidptosis and glycolysis related risk score signature for prediction of prognosis and ICI therapeutic responsiveness in colorectal cancer. Sci. Rep. 13(1), 13344 (2023). https://doi.org/10.1038/s41598-023-40381-5
15. Zhong, Q., et al.: Exploring the correlation of glycolysis-related chondroitin polymerizing factor (CHPF) with clinical characteristics, immune infiltration, and cuproptosis in bladder cancer. Am. J. Cancer Res. 13(6), 2213–2233 (2023)
16. Fearnhead, H.O., Vandenabeele, P., Vanden Berghe, T.: How do we fit ferroptosis in the family of regulated cell death? Cell Death Differ. 24(12), 1991–1998 (2017). https://doi.org/10.1038/cdd.2017.149
17. Tsvetkov, P., et al.: Copper induces cell death by targeting lipoylated TCA cycle proteins. Science 375(6586), 1254–1261 (2022). https://doi.org/10.1126/science.abf0529
18. Chen, L., et al.: Systemic analyses of cuproptosis-related lncRNAs in pancreatic adenocarcinoma, with a focus on the molecular mechanism of LINC00853. Int. J. Mol. Sci. 24(9), 7923 (2023). https://doi.org/10.3390/ijms24097923
19. Kuang, F., et al.: lncRNAs AC156455.1 and AC104532.2 as biomarkers for diagnosis and prognosis in colorectal cancer. Dis. Markers 2022, 4872001 (2022). https://doi.org/10.1155/2022/4872001
20. Zhang, Y., et al.: SNHG7 accelerates cell migration and invasion through regulating miR-34a-Snail-EMT axis in gastric cancer. Cell Cycle 19(1), 142–152 (2020). https://doi.org/10.1080/15384101.2019.1699753
21. Zheng, Q., et al.: FENDRR: a pivotal, cancer-related, long non-coding RNA. Biomed. Pharmacother. 137, 111390 (2021). https://doi.org/10.1016/j.biopha.2021.111390
22. Yang, F., Sun, S., Yang, F.: Prognostic and predicted significance of FENDRR in colon and rectum adenocarcinoma. Front. Oncol. 11, 668595 (2021). https://doi.org/10.3389/fonc.2021.668595
23. He, Z., et al.: The FENDRR/miR-214-3P/TET2 axis affects cell malignant activity via RASSF1A methylation in gastric cancer. Am. J. Transl. Res. 10(10), 3211–3223 (2018)
24. Xu, Y., Zou, X., Mei, J.: The risk correlation between N7-methylguanosine modification-related lncRNAs and survival prognosis of oral squamous

cell carcinoma based on comprehensive bioinformatics analysis. Appl. Bionics Biomech. 2022, 1666792 (2022). https://doi.org/10.1155/2022/1666792
25. Feng, Q., et al.: Autophagy-related long non-coding RNA signature for potential prognostic biomarkers of patients with cervical cancer: a study based on public databases. Ann. Transl. Med. 9(22), 1668 (2021). https://doi.org/10.21037/atm-21-5156
26. Zhang, X., et al.: The somatic mutation landscape and RNA prognostic markers in stomach adenocarcinoma. OncoTargets Ther. 13, 7735–7746 (2020). https://doi.org/10.2147/ott.s263733
27. Duan, L., et al.: Identification of autophagy-related LncRNA to predict the prognosis of colorectal cancer. Front. Genet. 13, 906900 (2022). https://doi.org/10.3389/fgene.2022.906900
28. Wei, J., et al.: An autophagy-related long noncoding RNA signature contributes to poor prognosis in colorectal cancer. J. Oncol. 2020, 4728947 (2020). https://doi.org/10.1155/2020/4728947
29. Bauden, M., et al.: Circulating nucleosomes as epigenetic biomarkers in pancreatic cancer. Clin. Epigenetics 7(1), 106 (2015). https://doi.org/10.1186/s13148-015-0139-4
30. Burgess, R.J., Zhang, Z.: Histone chaperones in nucleosome assembly and human disease. Nat. Struct. Mol. Biol. 20(1), 14–22 (2013). https://doi.org/10.1038/nsmb.2461
31. Hata, T., et al.: MUC1-C activates the NuRD complex to drive dedifferentiation of triple-negative breast cancer cells. Cancer Res. 79(22), 5711–5722 (2019). https://doi.org/10.1158/0008-5472.can-19-1034
32. Xu, Y., et al.: WERAM: a database of writers, erasers and readers of histone acetylation and methylation in eukaryotes. Nucleic Acids Res. 45(D1), D264–D270 (2017)
33. Benayed, R., et al.: High yield of RNA sequencing for targetable kinase fusions in lung adenocarcinomas with No mitogenic driver alteration detected by DNA sequencing and low tumor mutation burden. Clin. Cancer Res. 25(15), 4712–4722 (2019). https://doi.org/10.1158/1078-0432.ccr-19-0225
34. Lenz, H.J., Kahn, M.: Safely targeting cancer stem cells via selective catenin coactivator antagonism. Cancer Sci. 105(9), 1087–1092 (2014). https://doi.org/10.1111/cas.12471
35. Campbell, H., et al.: Δ133p53 isoform promotes tumour invasion and metastasis via interleukin-6 activation of JAK-STAT and RhoA-ROCK signalling. Nat. Commun. 9(1), 254 (2018). https://doi.org/10.1038/s41467-017-02408-0
36. Cinausero, M., et al.: KRAS and ERBB-family genetic alterations affect response to PD-1 inhibitors in metastatic nonsquamous NSCLC. Ther. Adv. Med. Oncol. 11, 1758835919885540 (2019). https://doi.org/10.1177/1758835919885540
37. Yi, D., et al.: Germline TP53 and MSH6 mutations implicated in sporadic triple-negative breast cancer (TNBC): a preliminary study. Hum. Genomics 13(1), 4 (2019). https://doi.org/10.1186/s40246-018-0186-y
38. Snyder, A., et al.: Genetic basis for clinical response to CTLA-4 blockade in melanoma. N. Engl. J. Med. 371(23), 2189–2199 (2014). https://doi.org/10.1056/nejmoa1406498
39. Rizvi, N.A., et al.: Cancer immunology. Mutational landscape determines sensitivity to PD-1 blockade in non-small cell lung cancer. Science 348(6230), 124–128 (2015). https://doi.org/10.1126/science.aaa1348
40. Luo, L., et al.: A necroptosis-related lncRNA-based signature to predict prognosis and probe molecular characteristics of stomach adenocarcinoma. Front. Genet. 13, 833928 (2022). https://doi.org/10.3389/fgene.2022.833928
41. Zhu, Z., et al.: Comprehensive analysis of cuproptosis-related lncRNAs to predict prognosis and immune infiltration characteristics in colorectal cancer. Front. Genet. 13, 984743 (2022). https://doi.org/10.3389/fgene.2022.984743
42. Song, W., et al.: N6-Methyladenosine-Related lncRNA signature predicts the overall survival of colorectal cancer patients. Genes 12(9), 1375 (2021). https://doi.org/10.3390/genes12091375
43. Zeng, H., et al.: Construction and analysis of a colorectal cancer prognostic model based on N6-methyladenosine-related lncRNAs. Front. Cell Dev. Biol. 9, 698388 (2021). https://doi.org/10.3389/fcell.2021.698388
44. Nie, F., et al.: Role of Raf-kinase inhibitor protein in colorectal cancer and its regulation by hydroxycamptothecine. J. Biomed. Sci. 22(1), 56 (2015). https://doi.org/10.1186/s12929-015-0162-y
45. Javed, B., Mashwani, Z.U.: Synergistic effects of physicochemical parameters on bio-fabrication of mint silver nanoparticles: structural evaluation and action against HCT116 colon cancer cells. Int. J. Nanomedicine 15, 3621–3637 (2020). https://doi.org/10.2147/ijn.s254402
46. Cheng, C., et al.: FENDRR sponges miR-424-5p to inhibit cell proliferation, migration and invasion in colorectal cancer. Technol. Cancer Res. Treat. 19, 1533033820980102 (2020). https://doi.org/10.1177/1533033820980102
47. Liu, J., Yuan, J.F., Wang, Y.Z.: METTL3-stabilized lncRNA SNHG7 accelerates glycolysis in prostate cancer via SRSF1/c-Myc axis. Exp. Cell Res. 416(1), 113149 (2022). https://doi.org/10.1016/j.yexcr.2022.113149
48. Pei, L.J., et al.: LncRNA-SNHG7 interferes with miR-34a to de-sensitize gastric cancer cells to cisplatin. Cancer Biomark. 30(1), 127–137 (2021). https://doi.org/10.3233/cbm-201621
49. Chen, S., Shen, X.: Long noncoding RNAs: functions and mechanisms in colon cancer. Mol. Cancer 19(1), 167 (2020). https://doi.org/10.1186/s12943-020-01287-2

## SUPPORTING INFORMATION

Additional supporting information can be found online in the Supporting Information section at the end of this article.

**How to cite this article:** Fan, Q., et al.: Analysis of disulfidptosis- and cuproptosis-related LncRNAs in modulating the immune microenvironment and chemosensitivity in colon adenocarcinoma. IET Syst. Biol. 18(2), 55–75 (2024). https://doi.org/10.1049/syb2.12089